Strong impacts on aerosol indirect effects from historical oxidant changes

Inger Helene Hafsahl Karset[1], Terje Koren Berntsen[1,2], Trude Storelvmo[3], Kari Alterskjær[2], Alf Grini[4], Dirk Olivié[4], Alf Kirkevåg[4], Øyvind Seland[4], Trond Iversen[4], and Michael Schulz[4]

[1]University of Oslo, Department of Geosciences, Section for Meteorology and Oceanography
[2]CICERO Center for International Climate Research, Oslo, Norway
[3]Yale University, Department of Geology and Geophysics, New Haven, USA
[4]Norwegian Meteorological Institute, Oslo, Norway

Correspondence to: Inger Helene Hafsahl Karset (i.h.h.karset@geo.uio.no)

Abstract. Uncertainties in effective radiative forcings through aerosol-cloud interactions (ERF$_{aci}$, also called aerosol indirect effects) contribute strongly to the uncertainty in the total preindustrial-to-present-day anthropogenic forcing. Some forcing-estimates of the aerosol indirect effects are so negative that they even offset the greenhouse gas forcing. This study highlights the role of oxidants in modeling of the preindustrial-to-present-day aerosol indirect effects. We argue that the aerosol precursor

5   gases should be exposed to oxidants of its era to get a more correct representation of secondary aerosol formation. Our model simulations show that the total aerosol indirect effect changes from -1.32 Wm^{-2} to -1.07 Wm^{-2} when the precursor gases in the preindustrial simulation are exposed to preindustrial instead of present-day oxidants. This happens because of a brightening of the clouds in the preindustrial simulation, mainly due to large changes in the nitrate radical (NO$_3$). The weaker oxidative power of the preindustrial atmosphere extends the lifetime of the precursor gases, enabling them to be transported higher up

10   in the atmosphere and towards more remote areas where the susceptibility of the cloud albedo to aerosol changes is high. The oxidation changes also shift the importance of different chemical reactions and produce more condensate, thus increasing the size of the aerosols and making it easier for them to activate as cloud condensation nuclei.

1 Introduction

It is well established that changes in atmospheric aerosol abundance since pre-industrial times have had a strong, albeit un-

15   certain, influence on Earth's climate over the last century. Atmospheric aerosols are not just impacting climate by directly absorbing and reflecting radiation, but also indirectly by acting as cloud condensation nuclei (CCN) and ice nuclei (IN). Through cloud albedo increases mediated by enhancements of CCN, aerosols brighten the clouds and enhance their cooling effect by increasing the reflection of incoming solar radiation (Twomey, 1977). More numerous cloud droplets may also alter rain formation mechanisms, thus the cooling effect could be further enhanced by suppressed precipitation followed by increased

20   cloud lifetime, cloud amount and cloud extent (Albrecht, 1989; Pincus and Baker, 1994). The impact of IN changes remains uncertain (Storelvmo, 2017; Lohmann, 2017).

Aerosol indirect effects on Earth's radiation budget are often quantified in terms of their effective radiative forcing (Myhre et al., 2013). Unlike instantaneous radiative forcing, effective radiative forcing includes effects from rapid tropospheric adjustments (Boucher et al., 2013). Otherwise, it does not include any feedbacks in the climate system. Model studies of the direct and indirect effects typically carry out two simulations, with aerosols and aerosol precursor gases from preindustrial times

5 (PI) and present-day (PD), respectively. The difference in cloud forcing, measured as effective radiative forcing between the two simulations, represents the aerosol indirect effects if the direct aerosol effect in cloudy skies is negligible (Ghan, 2013). Results from several model studies show that this number varies considerably. To what extent aerosol-cloud interactions have contributed to the global radiative forcing in the anthropocene remains highly uncertain and continues to be a research topic of much interest. (Lohmann, 2017) shows that model estimates of $ERF_{ari+aci}$ (ari: aerosol-radiation interactions. aci: aerosol-cloud

10 interactions) vary from -0.07 to -3.41 Wm^{-2}, while the latest Assessment Report (AR5) from the Intergovernmental Panel on Climate Change (IPCC) gives an expert judgement of $ERF_{ari+aci}$ of -0.9 Wm^{-2}, with a 5 to 95 % uncertainty range of -1.9 to -0.1 Wm^{-2} mostly coming from the uncertainties in the aci-component (Boucher et al., 2013). Uncertainties in the natural background emissions have been highlighted as a large contributor to the uncertainty in the indirect effects (Lohmann et al., 2000; Kirkevåg et al., 2008; Hoose et al., 2009; Carslaw et al., 2013), while Gettelman (2015) pointed out that its sensitivity to

15 parameterizations of microphysical processes in global models are even higher. In this study, we examine a third factor, namely the oxidants involved in forming aerosols.

Aerosols may enter the atmosphere directly, or they can be formed after in situ oxidation of precursor gases to condensable species (Seinfeld and Pandis, 2016). The oxidation process yields secondary gases with lower saturation vapor pressure, which allows them to either condense on already existing particles or nucleate into new particles under atmospheric conditions. Both

20 processes depend on the amount of emitted precursor gases, but also on the atmospheric oxidation capacity. While model studies of PD-PI aerosol indirect effects usually point out that they use different emissions of aerosols and aerosol precursor gases for the two different time periods, the choice of oxidant levels is usually not specified (Lohmann and Diehl, 2006; Menon and Rotstayn, 2006; Hoose et al., 2008; Storelvmo et al., 2008; Lohmann, 2008; Lohmann and Ferrachat, 2010; Wang et al., 2011; Yun and Penner, 2013; Neubauer et al., 2014; Gettelman, 2015; Gettelman et al., 2015; Tonttila et al., 2015; Sant

25 et al., 2015). A notable exception is Salzmann et al. (2010), who use different oxidant levels for the different eras. Personal communication with scientists from different modelling groups confirms that it is common to use PD-oxidants for both PD and PI simulations (U. Lohmann, C. Hoose, A. Kirkevåg, A. Gettelman, D. Neubauer, personal communication 2017).

Human activity has influenced the oxidant level mainly through increased emissions of CO, NO_x, and CH_4 from fossil fuel combustion, biomass burning and the use of fertilizers in agriculture (Crutzen and Lelieveld, 2001). Due to this anthropogenic

30 activity, precursor gases emitted into the PI atmosphere were exposed to a different oxidant level than the gases emitted today, implying a difference in the rate and distribution of new particle formation in the atmosphere. The aim of this study is to quantify this difference and to give a more realistic estimate of the PD-PI indirect effect by letting the precursor gases in the PI-simulation be exposed to an oxidant level that is representative for its era.

Due to counteracting effects, the sign and magnitude of the global mean historical oxidant change is uncertain (Naik et al.,

35 2013a, b; Murray et al., 2014). While in a low NO_x-regime, CO and CH_4 act as sinks for the hydroxyl radical (OH), one

of the most important oxidants in the troposphere, the opposite is the case in a high NO_x-regime (Collins et al., 2002). As a consequence, OH has experienced an increase in polluted areas where the NO_x level is high, while it has decreased in remote areas where the NO_x-level is low and the CH_4 level is high due to their different lifetimes (Wang and Jacob, 1998; Prinn, 2003). The situation is different for ozone (O_3), where an increase in NO_x, CO or CH_4 usually favours O_3-production in both low and

5   high NO_x regimes (Seinfeld, 1989; Chameides et al., 1992). This also holds for the NO_3 radical, which is produced through reactions between NO_x and O_3 (Wayne et al., 1991) and probably was present at lower levels everywhere in preindustrial times.

Difficulties in measuring the oxidants has resulted in limited information about the atmospheric oxidant level, especially before the industrial era (Pavelin et al., 1999). Despite this limitation, results from model simulations based on information about emission changes, in combination with the few oxidant measurements that exist, give an indication of how the oxidative

10   power of the atmosphere has changed since preindustrial time (Prinn, 2003; Berntsen et al., 1997; Wang and Jacob, 1998; Tsigaridis et al., 2006; Naik et al., 2013a, b; Young et al., 2013; Murray et al., 2014; Khan et al., 2015).

When trying to get a better understanding of the response of clouds to aerosol perturbations, or comparing this effect between models, the choice of oxidant level may not be important as long as there is consistency between the different models. However, the oxidant level may be important when the modelled preindustrial-to-present-day aerosol indirect effect is used as an estimate

15   of the contribution from aerosol-cloud interactions to the total forcing of climate change since PI, as was done in IPCC AR5. Recent global model estimates of the aerosol indirect effects do, to a larger extent than before, represent more of the gas to aerosol formation processes through oxidation followed by nucleation (Boucher et al., 2013; Lohmann, 2017), increasing the importance of understanding the effects and the model treatment of the oxidants. More and more models will also incorporate an interactive atmospheric gas phase chemistry in transient climate studies, making the characterisation of effective radiative

20   forcing a larger challenge. With this study we aim to use model simulations to investigate the impact on aerosol indirect effects from historical oxidants changes by letting the aerosol precursor gases in the PI-simulation be exposed to PI- instead of PD-oxidant levels.

2   Model

2.1   General description

25   The model used in this study is CAM5.3-Oslo (Kirkevåg et al., 2018), an updated version of the atmospheric component of the Norwegian Earth System Model (NorESM) (Bentsen et al., 2013; Iversen et al., 2013; Kirkevåg et al., 2013). CAM5.3-Oslo is based on the Community Atmospheric Model version 5.3 (Neale et al., 2012; Liu et al., 2016), but has its own aerosol module (OsloAero). It also includes other modifications, such as the implementation of heterogeneous ice nucleation (Wang et al., 2014; Hoose et al., 2010). OsloAero has 21 aerosol tracers, distributed among six species (sulphate, secondary organic

30   aerosols (SOA), black carbon, organic matter, mineral dust and sea-salt), and four precursor gases (SO_2, dimethyl sulfide (DMS), isoprene and monoterpene). DMS-emissions are wind-driven based on Nightingale et al. (2000), emissions of SO_2 are interpolated from prescribed monthly mean decadal climatology given by Lamarque et al. (2010). The emissions of the Biogenic Volatile Organic Compounds (BVOC) isoprene and monoterpene are calculated online every timestep of half an

hour by a satellite phenology version of the Community Land Model version CLM4.5 (Oleson et al., 2013), using the Model of Emissions of Gases and Aerosols from Nature version 2.1 (MEGAN2.1) (Guenther et al., 2012), where the emissions are impacted by both radiation and temperature, inducing a diurnal variation. The aerosol nucleation is based on Makkonen et al. (2014), with improvements described in Kirkevåg et al. (2018), which includes nucleation of both SO_4 and SOA. The stratiform

5   clouds are treated by the two-moment bulk microphysics scheme, MG1.5, that is almost identical to MG1 described in Morrison and Gettelman (2008), but with cloud droplet activation moved before the cloud microphysical process rates (Gettelman, 2015; Gettelman and Morrison, 2015).

Methods by Ghan (2013) are used for calculating the effective radiative forcing of aerosols. The part called "cloud radiative forcing", or ΔC_{clean} is often used as a measure of aerosol indirect effects, where it represents the difference in the top of the

10   atmosphere cloud forcing between simulations performed with different aerosols. ΔC_{clean} also includes semi-direct effects, but additional simulations with non-absorptive aerosols have shown that this term is negligible compared to the indirect effects in the model (Kirkevåg et al., 2018). Henceforth we use ΔC_{clean} as a measure of aerosol indirect effects in this study.

2.2   Oxidant chemistry

CAM5.3-Oslo includes simple chemistry for sulfur and SOA species, which makes use of the chemical preprocessor MOZART

15   (Emmons et al., 2010) modified for the CAM framework (Liu et al., 2012). The preprocessor is a numerical scheme that generates code to the model based on some input chemical reactions and rates. The generated code provides information of how the chemical tracers evolve as a function of concentration of chemical species. Reactions (R1-R10) in Table 1 represent the gas phase oxidation of the precursor gases in the model. SOA_{LV} and SOA_{SV} are both gaseous SOA (SOA(g)), low volatile and semi-volatile respectively, where only the former can take part in nucleation, while both can condense on already existing

20   aerosols. While (R2) represents the H abstraction part of the complex reaction where DMS is oxidized by OH, (R3) represents the OH addition part. At standard conditions (temperature of 273.13 K and pressure of $1.013 \cdot 10^5$ hPa), the ratio between the reaction rates of (R2) and (R3) is 7/13 (R2/R3). Methanesulfonic acid (MSA) is produced in (R3) following Chin et al. (1996). Since CAM5.3-Oslo does not trace MSA, the product is put in the SOA-tracers, since MSA can contribute to aerosol formation and growth (Bork et al., 2014). The oxidation of biogenic volatile organic compounds (BVOC) in (R5-R10) are based on

25   Makkonen et al. (2014), but with some extensions explained by Kirkevåg et al. (2018). The model also includes aqueous phase oxidation of SO_2 by H_2O_2 and O_3 (Tie et al., 2001; Neale et al., 2012). H_2O_2 production and loss are calculated online through reactions (R11-R13) in Table 1.

The concentrations of the other oxidants (NO_3, O_3, OH and HO_2) are prescribed by interpolated monthly mean values produced by a global model with full chemistry (Lamarque et al., 2010). PD and PI values used in this study are taken from

30   decadal climatologies around year 2000 and 1855 respectively, and the percent change in the annual mean values can be seen in Fig. 1. NO_3 experiences a very large relative change between PI and PD (up to more than 1000 % in the northern hemisphere), which is also seen in other model studies (Khan et al., 2015). CAM5.3-Oslo also applies a daily cycle to OH and HO_2, which is not included in CAM5.3. The prescribed oxidants in Fig. 1 are only applied in the chemistry of the model, and not for radiation

calculations. O_3 is also important for radiation calculations, but here another prescribed O_3-field is applied, which is the same in both PI and PD.

2.3 Configurations

The model was configured with a horizontal resolution of 0.9° (latitude) by 1.25° (longitude) and 30 hybrid levels between
5   the surface and ~3 hPa. The simulations were carried out using nudged meteorology produced by the model itself to constrain the natural variability (Kooperman et al., 2012). The horizontal wind components (U, V) were nudged with a relaxation time scale of six hours, while the temperature was allowed to run free, enabling impacts by aerosol perturbations, which could be important when calculating indirect effects (Zhang et al., 2014). Prescribed climatological SSTs and sea-ice extent from the mean of 1982-2001 were used in all simulations, as well as greenhouse gases and land use information from year 2000.

10 ## 3 Experimental setup

3.1 General

Figure 2 shows an overview of how the simulations were carried out. The model was first run for six years to output instantaneous meteorological data. This simulation used PD-conditions for all possible choices. All other simulations were nudged to the meteorology of this simulation. For each modification to the default model setup, three different simulations were carried
15   out. These three simulations used the prescribed precursor- and aerosol emissions and oxidant concentrations given in Table 2. Each of them was restarted from an already spun up case with emissions and oxidants from its era. The last three years of the simulations were analyzed. The first set of simulations used CAM5.3-Oslo as described above, without any other modifications to the code. We name these simulations ORG, and the impact of historical oxidant changes on the PD-PI indirect effects in CAM5.3-Oslo are quantified by the difference we get (relative to the PD simulation PDAER_PDOXI_ORG) when switching
20   between the two PI-simulations PIAER_PDOXI_ORG and PIAER_PIOXI_ORG.

3.2 Decomposing the oxidant change

To estimate the importance of the different changes in the individual oxidants between PI and PD, four additional simulations with PI-aerosols were carried out. In these simulations, the oxidant of interest was changed to PI-concentrations, while all other oxidants were kept at PD-levels. Acknowledging the complexity of oxidant chemistry, one can not expect that separate oxidant
25   changes in separate simulations will add up to the same result as changing them all simultaneously. To explore the importance of this non-linearity, another four additional simulations were performed, keeping all oxidants from PI except for the one of interest, which was set to PD-levels.

4 Results and discussion

4.1 Original setup

The top panels of Fig. 3 show the PD-PI indirect effect for shortwave radiation (a), longwave radiation (b), and total radiation (c) when using the standard setup with PD-oxidants in both simulations. The bottom panels of Fig. 3 show the impact of

5 historical oxidant changes on the PD-PI indirect effect. Figure 3(d) shows that letting the precursor gases in the PI-simulation be exposed to oxidants from its era, instead of oxidants from PD, makes the shortwave indirect effect 0.39 Wm^{-2} less negative (changing from -1.48 Wm^{-2} to -1.09 Wm^{-2}). This implies that the clouds in the PI-simulation with PI-oxidants are cooling the climate more through SW-effects than the clouds in the PI-simulation with PD-oxidants, reducing the difference in shortwave cloud forcing between PI and PD. Figure 3(e) shows that the change in longwave indirect effect is -0.14 Wm^{-2} (from 0.16

10 Wm^{-2} to 0.02 Wm^{-2}), meaning that the clouds in the PI-simulation with PI-oxidants are warming the climate more through increased absorption of longwave radiation, reducing the difference in longwave cloud forcing between PI and PD. Figure 3(f) shows a total (shortwave + longwave) change in the indirect effects of +0.25 Wm^{-2} (changing from -1.32 Wm^{-2} to -1.07 Wm^{-2}), meaning that the PI-clouds with PI-oxidants are cooling the climate more than the PI-clouds with PD-oxidants, thus making the indirect effect less negative. The largest changes in the shortwave indirect effect occur over ocean, especially over

15 the North Pacific, off the west coast of America, in remote areas between $30°$ S and $60°$ S and over the Indian Ocean. The changes in the longwave indirect effect mainly take place in the polar regions and over the Indian Ocean.

Different cloud- and aerosol changes can help explain the resulting change in the indirect effect. Some of these are presented in Fig. 4. In the global mean, switching to PI-oxidants in the PI-simulation results in (a) more numerous aerosol particles (+9.2 %), (b) more numerous cloud droplets (CDNC) (+3.7 %), (c) smaller cloud droplets (-1.5 %), (d) larger cloud fraction (+0.26

20 %), which is mainly caused by changes in the low cloud fraction, and (e) larger total gridbox averaged liquid water path (LWP) (+1.7 %). The size of the cloud droplets in Fig. 4(c) is taken from the cloud top layer of the stratiform clouds.

The sign of the changes in the global mean cloud and radiative properties seen in Figs. 3 and 4 is as expected for an increase in the global mean aerosol number concentration. We will now further investigate why the oxidant changes enhance the aerosol number concentration. Figures 3 and 4 show that the distribution of the changes in aerosol number concentration does not

25 always correspond directly to the distribution of the changes in the cloud and radiative properties. This indicates that it is not only the change in aerosol number concentration that is important for the result, but also changes in the composition of the aerosols and in the atmospheric conditions where the aerosol changes take place.

4.1.1 The increase in aerosol number concentration

Since the formation of new aerosols depends on the availability of low volatile gases, and the PI-atmosphere consisted of

30 relatively small amounts of oxidants to produce secondary gases with reduced volatility, one could expect a reduction in the aerosol number concentration when switching from PD- to PI-oxidants. This is the opposite of what Fig. 4(a) shows. The increased lifetime of the precursor gases and the aerosols seen in Table 3 partly explain this. When the oxidizing power of the atmosphere is reduced, the precursor gases with high volatility are transported higher up in the atmosphere before they

are oxidized. This is seen in Fig. 5, where the relative change in chemical loss of (a) DMS, (b) SO_2, (c) isoprene, and (d) monoterpene through oxidation is negative close to the surface, but positive higher up in the atmosphere when switching from PD- to PI-oxidants in the PI-simulation. This results in the change in the vertical profile of the aerosol number concentration seen in Fig. 8(a), with lower values close to the ground, but larger values above $\sim$900 hPa. Aerosols formed from gases higher

5 up in the atmosphere are not removed by dry- and wet-deposition as easily as aerosols formed closer to the ground, explaining the longer aerosol lifetime seen in Table 3 (Jaenicke, 1980; Williams et al., 2002).

It is not only the vertical transport of the gases that changes. The reduced oxidation capacity also increases the horizontal transport of the primary precursors away from the source regions. This is seen in Fig. 6, focusing on DMS, the main precursor gas over ocean, where most of the aerosol-, cloud- and radiation changes occur. Figure 6(a) shows the distribution of DMS-

10 emissions, which is equal in all PI-simulations, while Fig. 6(b) shows the change in the net chemical loss of DMS through oxidation when switching from PD- to PI-oxidants. Increased horizontal transport happens from areas with negative values to areas with positive values, since chemical loss through oxidation is the only way DMS can be lost in the model. The increase is especially pronounced in the North Pacific, with increased transport further south and towards the Arctic, but is also found in the southern oceans with increased transport from the large emission sources close to the coast and towards the remote ocean.

15 Figure 6(c) shows that this transport results in increased aerosol formation close to the ground in areas that receive more DMS with PI-oxidants. Since the precursor gases are spread more in space with PI-oxidants, towards more remote areas where the background concentration of aerosols are low, the coagulation sink during the nucleation process is reduced, contributing to an increase in the formation rate. In CAM5.3-Oslo, "formation rate" describes the formation of aerosol particles of 12 nm, which is the size limit a particle must achieve to be accounted for in the aerosol number concentration (Figs. 4(a) and 6(e)). "Nucleation

20 rate" describe the formation of aerosol particles of 2 nm. As for all other aerosols, the particles between 2 and 12 nm can also be lost through coagulation with background aerosols. Figure 6(d) shows how the coagulation sink of these particles changes when switching from PD- to PI-oxidants in the PI-simulation. The reduction in the coagulation sink is especially large close to the strong DMS-emissions sources (Fig. 6(d)). The areas over ocean with increased formation rate close to the ground corresponds well with the areas in Fig. 6(e) with increased aerosol number concentrations, indicating that the horizontal

25 transport of DMS due to its longer lifetime in an atmosphere with PI-oxidants is important for the increase in aerosol number concentration. Higher up in the atmosphere (above $\sim$850 hPa), the formation rate of aerosols also increase over the emission sources and at higher latitudes (not shown). The change in the total vertically integrated coagulation sink decreases by 17.7 % when switcing from PD- to PI-oxidants in the PI-simulation, favouring enhanced formation of new aerosols. Increased lifetime of the precursor gases also results in an increased deposition rate of SO_2 of 12.8 % (DMS, isoprene and monoterpene are only

30 lost through atmospheric chemistry), favouring a decrease in the formation of new aerosols. As a result of these two competing effects, the total vertically integrated formation of new aerosols increases by 5.4 %.

4.1.2 The increase in cloud droplet number concentration

Figure 4(b) shows that the CDNC increases in regions that experience large relative changes in the aerosol number concentration (Fig. 4(a)). The aerosol and CDNC increases are linked to the extended DMS lifetime discussed above (Fig. 6(b)),

which in turn allows for more DMS transport to and subsequently increased aerosol formation in remote regions like the South Pacific (SP) and the Arctic Ocean (AO), as defined in Fig. 7. The region named North Pacific (NP) in Fig. 7 experiences a local minimum in the change in the aerosol number concentration. Figure 6 shows that this is caused by less aerosol formation in this region. Nevertheless, NP also experiences a relatively large increase in CDNC. The vertical profiles in Fig. 8 show that

5 the regions which receive more precursor gases with PI-oxidants (AO and SP) experience an increase in both aerosol number concentration and CDNC for all altitudes, while the NP region experiences a decrease close to the ground, but an increase higher up. The latter can be explained by the vertical shift in the oxidation (Fig. 5). In NP, the height above which the change in CDNC is positive is located lower down in the atmosphere than the height at which the aerosol number concentration starts to increase (Fig. 8(i) and 8(l)). This can be explained by the change in the size of the aerosols (Fig. 8(j)), caused by the increased

10 aerosol condensate relative to the aerosol number concentration (Fig. 8(k)). The mean size of the aerosols is calculated as a mean of the number mean radius of all mixtures in the model, weighted by the number of aerosols in each mixture. The relative amount of condensate increases in the global mean (Fig. 8(c)) and in the northern hemisphere (Fig. 8(g) and 8(k)) because of the strong shift in the importance of the different oxidation reactions (Fig. 9). Both DMS, isoprene, monoterpene and SO_2 have the potential of being oxidized in three different ways. Figure 9 shows how many percent of the oxidant reactions of a specie

15 happening through the different reactions. The largest change in the oxidant level when switching from PD- to PI-oxidants is found for NO_3 in the northern hemisphere (Fig. 1(c)). When switching to PI-oxidants, the relative fraction of DMS oxidized by NO_3 is reduced (Fig. 9(a,c,d), red curves), while the the oxidation fraction involving the other oxidants become more important. For the dominant precursor gas over the remote oceans, DMS, this means that instead of mostly getting $1 \cdot SO_2$ and no SOA out off a DMS-oxidation through the reaction (R4), the PI-atmosphere will to a larger extent produce $0.75 \cdot SO_2$ and

20 some SOA (R3). SO_2 nucleates easier than SOA, and 80 % of the SOA from (R3) comes as SOA_{SV}, which is only allowed to condense. The change in aerosol size in SP (Fig. 8(n)) deviates from the other regions. This is due to the increase in OH in SP when switching to PI-oxidants (blue colors in Fig. 1(a)), giving rise to enhanced nucleation of small SO_4-aerosols followed by an enhanced H_2SO_4-production through (R1). This also happens in AO, where the OH-level also is larger in PI, but here this effect is small relative to the effect of the increased SOA_{SV}-production due to the large NO_3-change in the northern hemisphere

25 (Fig. 1(c)).

4.1.3 The change in aerosol indirect effect

The SW radiative effect of a change in CDNC varies depending on where these changes take place. Twomey (1991) showed that dA/d(CDNC), where A is the cloud albedo, is largest in clean regions with low CDNC and where the cloud albedo is approximately 0.5. The SW radiative effect will also be larger in areas with low surface albedo, in areas close to the equator

30 due to more incoming solar radiation, and in areas where the cloud fraction is high. The last two factors, in addition to the factors in Twomey (1991), are taken into account in Eq. (6) in Alterskjær et al. (2012) when finding a cloud-weighted susceptibility function. This is a hybrid between the simplified dA/d(CDNC) of Twomey and the more complex d(ERFaci)/d(CDNC), which we see in Figure 3. It only includes the first aerosol indirect effect, and not second aerosol indirect effects (such as increased lifetime, cloud amount and cloud extent). The susceptibility function will give an indication of which areas over

ocean being relatively more susceptible than others to cloud albedo changes caused by changes in CDNC. The cloud-weighted susceptibility function is normalized by its maximum value. Applying this function to three years of daily output from the PIAER_PDOXI_ORG-simulation in this study results in Fig. 10(a). Areas with high cloud-weighted susceptibility are found off the west coast of the continents and in the remote southern ocean storm tracks. The large increase in CDNC (Fig. 4(b)) in

5 the North and South Pacific regions efficiently increase the albedo of the clouds, thus resulting in the large change in the SW indirect effect seen in Fig. 3(d). Due to less insolation in the Arctic, the cloud-weighted susceptibility in this region is low, resulting in a negligible effect on the SW indirect effect, even though this is the region that experiences the relatively largest increase in both CDNC (Fig. 4(b)), cloud fraction (Fig. 4(d)) and LWP (Fig. 4(e)) due to the oxidant changes. The LW indirect effect is not dependent on the incoming solar radiation, so the large changes in cloud properties seen in the Arctic affect the LW

10 indirect effect. The thicker and longer-lived clouds in the simulation with PI-oxidants act to reduce the difference in LW heating between the PD- and PI-simulations (Fig. 3(e)). Figure 10(b) shows the vertical profile of the global mean cloud-weighted susceptibility. It shows that the decrease in CDNC close to the ground (Fig. 8(d)) does not affect the cloud albedo as much as the increase in CDNC between 900 and 800 hPa.

4.2 Decomposing the oxidant change

15 To get a better understanding of the results in the original experiment, results from the sensitivity tests where only one oxidant at a time was changed are analyzed. Figure 11 shows differences in the global mean shortwave and longwave indirect effect between the setups with modified PI-simulations (PIOXI, PIOH, PIO3, PINO3 and PIHO2) and the original setup with only PD-oxidants in both simulations. Figure 12 shows the same for the horizontal distribution. Changing only NO_3 (PINO3) gives almost the same result as changing all of the oxidants (PIOXI), indicating that the historical change in NO_3 is the most

20 important oxidant change for indirect effect calculations. This corresponds well with Fig. 1 showing that NO_3 is the oxidant that has experienced the largest relative change since PI, and Fig. 9 showing that the importance of the oxidation reactions involving NO_3 drop the most when switching from PD- to PI-oxidants in the PI-simulation. The negative pattern over land in the tropics in PINO3 that is missing in PIOXI (Fig. 12) seems to be explained by the changes in O_3. Analysis of the PIO3-simulation shows that replacing only the O_3-oxidant with PI-values reduces the importance of (R6) where monoterpene is oxidized by

25 O_3 giving SOA_{LV}, while the other oxidation reactions of monoterpene giving SOA_{SV} become more important. This results in less new aerosol formation and increased growth of the already existing aerosols through condensation, increasing the CCN-concentration and the following cloud droplet activation and CDNC.

Table 4 shows that there are some non-linearities associated with changing one oxidant at a time. The odd numbered rows show the impact on the indirect effects when changing one oxidant at a time, while the even rows show the difference in

30 the effect of changing all oxidant and changing all except for one oxidant. If there were no non-linearities involved in the oxidant chemistry, a odd numbered row and the following row would have shown the same numbers. This is not the case, but the differences are relatively small, supporting the indication that the contributions to the total result mainly stem from the historical changes in NO_3.

4.3 Sensitivity tests

Due to nonlinear processes and feedbacks in the model, it is difficult to separate the different effects and to estimate how much each of them contributes to the final result. As an example, enhanced formation of new aerosols can be explained as in Sect. 4.1.1, starting by the increase in lifetime of the precursor gases, but the enhanced importance of reactions giving

5   SOA sufficiently with low volatility to nucleate new aerosols ((R3) and (R6)) can also be a part of the explanation. To get a better understanding of the importance of the various factors and processes, extra sensitivity tests with four new setups were carried out, all of them consisting of three different simulations, as illustrated in Fig. 2, all deviating from the original set-up as well as from Kirkevåg et al. (2018), either through changes in some of the chemical reactions (R1-R10), or directly through manipulating the aerosol input to the code for cloud droplet activation. Information about the setup for the sensitivity tests are

10 found in Table 5.

4.3.1 NOSOALVDMS and NOSOALVBVOC

When moving from a high NO_3-regime (PD-oxidants) to a low NO_3-regime (PI-oxidants), the oxidation reactions giving SOA_{LV} as a product ((R3) and (R6)) become more important. This is seen from the large change in the global mean column burden of SOA_{LV} (+49.6 %). Since SOA_{LV} can take part in nucleation and give rise to the increased aerosol concentration seen

15 in Fig. 4(a), the additional SOA_{LV} that is produced when using PI-oxidants may explain the change in the indirect effects seen in Fig. 3. When replacing all of the originally produced SOA_{LV} from the DMS-oxidation in (R3) with SOA_{SV}, the change in the total aerosol indirect effects is almost the same as for the original setup (ΔAIE_{tot}: +0.25 Wm^{-2}), and the geographical pattern looks largely the same (not shown here). This also holds when doing the same for the oxidation of monoterpene (R6) (ΔAIE_{tot}: +0.26 Wm^{-2}). The pattern of the resulting AIE from the oxidant changes in the NOSOALVBVOC-simulations looks almost

20 the same as for the original simulations, except over the Amazon where the signal from the O_3-changes explained in the last section is gone. This does not change the global mean AIE by more than 0.01 Wm^{-2}, however. These sensitivity tests indicate that even though the global mean burden of SOA_{LV} changes a lot when using PI-oxidants, this plays a minor role for the change in the indirect effects seen in Fig. 3.

4.3.2 NOSOA

25 The increased production of total SOA(g) (SOA_{SV} and SOA_{LV}) when switching from PD to PI-oxidants has potential to cause changes in the indirect effects even though the nucleation effect is negligible. All SOA(g) can condense onto already nucleated aerosols and make it easier for them to grow to the critical size for cloud droplet activation, except for cases where the reduction in hygroscopicity is more important than the increase in size. The impact of the hygroscopicity changes due to the changes in the oxidant levels has been tested and found to be negligible (not shown here). The change in total global mean column burden

30 of SOA(g) due to changes in the oxidant levels with the original setup was +40.7 %. To find out if this increase is causing the change in the indirect effects seen in Fig. 3, the model was run with the NOSOA-setup described in Table 5. This resulted in a change in the total aerosol indirect effects (ΔAIE_{tot}) of +0.14 Wm^{-2}, deviating by more than 0.10 Wm^{-2} from the original

setup. Removing products from the reaction makes the atmosphere cleaner, thus creating a different regime for both aerosol growth through reduced competition for condensable gases and for activation of aerosols through reduced competition for water vapor. This means that one cannot conclude that 0.11 Wm^{-2} of the 0.25 Wm^{-2} is caused by an increase in condensable SOA(g) when switching from PD- to PI-oxidants, but this sensitivity test indicates that it may have contributed to the overall

5 result seen in Fig. 3.

4.3.3 NACTOFF

This test is performed in order to see how important the change in the droplet activation on the smallest aerosols are. When modifying the oxidant level, the smallest aerosols are affected by the change in formation rate, while all aerosols are affected by the change in condensation. The results from this test give an indication of how important the changes associated with

10 the smallest aerosols are. When not allowing the smallest aerosols in mixture number 1 (corresponding to the nucleation mode in modal aerosol schemes) to activate, the change in the total aerosol indirect effects found when switching from PD- og PI-oxidants in the PI-simulation is small (ΔAIE$_{tot}$: -0.03 Wm^{-2}). This confirms that it is the difference in the number concentration of the smallest SO$_4$- and SOA-aerosols that gives the large difference in the indirect effect seen in Fig. 3.

5 Summary and conclusions

15 Here we have used the global atmospheric model CAM5.3-Oslo to study the effect of historical oxidant changes on the PD-PI aerosol indirect effect. The precursor gases in the PI-simulation were exposed to PI-oxidants instead of PD-oxidants. Our main findings are:

– The total aerosol indirect effect is reduced from -1.32 Wm^{-2} to -1.07 Wm^{-2}, mainly due to a cloud brightening in the modified PI-simulation.

20 – NO$_3$ is the oxidant that contributes the most to the changes.

– When the precursor gases are exposed to an atmosphere with relatively lower oxidative power (PI-oxidants vs. PD-oxidants), their lifetime increases and they are transported higher up in the atmosphere and horizontally towards more remote areas before they are oxidized and can contribute to new aerosol formation.

– A large portion of the new aerosol formation and the increase in aerosol number concentration occurs where the cloud-
25 weighted susceptibility is high, giving a large impact on the radiative effects.

– The change from PD- to PI-oxidants in the PI-simulation yields a shift in the chemical reactions towards increased production of condensate relative to the amount of gases that can nucleate, which increases the size of the aerosols, making it easier for them to activate.

Note, that the magnitude of the sensitivity of the total aerosol indirect effect to the choice of the oxidants in this study is as
30 large as the total sulfur direct forcing (Myhre et al., 2013), thus contributing significantly to the total preindustrial-to-present-

day anthropogenic forcing. Overviews of model results of the PD-PI aerosol indirect effect show occasionally so negative values that they even offset the warming from the greenhouse gases (Boucher et al., 2013; Lohmann, 2017). Our results suggest that such unrealistic cooling may appear less often if the precursor gases are exposed to oxidants of its era, instead of applying PD-oxidants for both PD- and PI-simulations.

5   The results in this study are only based on simulations from just one model, with its model-specific treatments of oxidants, aerosols, clouds and radiation that all include uncertainties and simplifications. This also holds for the single input dataset used for the prescribed oxidants. An evaluation of the extent to which uncertainties in the different schemes and in the prescribed oxidant fields affect the result is beyond the scope of this paper, but should be focus for future studies. The treatment of the MSA-product from DMS-oxidation by OH (R3) should be looked at in particular, since the changes in SOA-condensate from
10 that reaction seems to contribute to the resulting changes in the total aerosol indirect effects.

The impact of the oxidant changes also depend on the emissions of precursor gases in the model. Carslaw et al. (2013) show that there are large uncertainties linked to natural emissions, even when assuming that they do not vary between PI and PD. This was shown especially for DMS (Woodhouse et al., 2010), which is found to be one of the most important precursor gases in this study. Changes in temperature and pH in the ocean, changes in land use, insolation, CO_2 and more, may also have
15 contributed to a change in the emissions since preindustrial time (Charlsson et al., 1987; Guenther et al., 2012; Unger, 2014). CAM5.3-Oslo is also lacking some emissions that could be important for the magnitude of the effect of the oxidant changes, for example emissions of biogenic volatile organic compounds (BVOCs) from the ocean, which can contribute significantly to the marine aerosol loading (Shaw et al., 2010), creating a more polluted regime with the potential of different susceptibilities.

Despite the large uncertainties and simplifications mentioned above, we find that the treatment of the oxidants is open for
20 discussion. We suggest that a common way of treating the oxidants must be agreed upon when modeling aerosol effective radiative forcings. We also encourage other researchers to specify which oxidants are used in their studies of historical changes in aerosol-cloud interactions.

Simulations from the Aerosol Chemistry Model Intercomparison Project (AerChemMIP), endorsed by the Coupled-Model Intercomparison Project 6 (CMIP6) can be used to quantify preindustrial-to-present-day effective radiative forcings. Comparing
25 the cloud forcings from the simulations called piClim-aer and piClim-control (Collins et al., 2017) will be approximately the same as done in the original default setup in this study, with the same oxidant level in both simulations. For models without tropospheric chemistry, AerChemMIP does not include a setup that takes into account historical oxidant changes. However, models that include tropospheric chemistry can perform the simulation piClim-NTCF, which includes different ozone precursors in the two different simulations, giving different oxidation capacity. The piClim-NTCF simulation does not
30 include all the factors that contribute to the differences in the oxidant level between PD and PI (for example methane), but it includes some of them, so we suggest that a comparison of the cloud forcings in piClim-NTCF and piClim-control will facilitate calculations of the PD-PI aerosol indirect effect, including changes due to different oxidant levels, also for the CMIP6-models.

Competing interests.   The authors declare that they have no conflict of interest.

Acknowledgements. I. H. H. K., A. G., D. O., A. K., Ø. S., T. I. and M. S. have been financed by the research council of Norway (RCN) through the project EVA and the NOTUR/Norstore projects (Sigma2 account: nn2345k, Norstore account: NS2345K). We gratefully acknowledge Sara Marie Blichner and Moa Sporre for scientific discussions.

References

Albrecht, B. A.: Aerosols, cloud microphysics, and fractional cloudiness., Science, 245, 1227–1230, https://doi.org/10.1126/science.245.4923.1227, 1989.

Alterskjær, K., Kristjánsson, J. E., and Seland, O.: Sensitivity to deliberate sea salt seeding of marine clouds - Observations and model simulations, Atmospheric Chemistry and Physics, 12, 2795–2807, https://doi.org/10.5194/acp-12-2795-2012, 2012.

Bentsen, M., Bethke, I., Debernard, J. B., Iversen, T., Kirkevåg, A., Seland, Ø., Drange, H., Roelandt, C., Seierstad, I. a., Hoose, C., and Kristjánsson, J. E.: The Norwegian Earth System Model, NorESM1-M – Part 1: Description and basic evaluation, Geoscientific Model Development Discussions, 5, 2843–2931, https://doi.org/10.5194/gmdd-5-2843-2012, 2013.

Berntsen, T. K., A Isaksen, I. S., Myhre, G., Fuglestvedt, J. S., Stordal, F., Alsvik Larsen, T., Freckleton, R. S., and Shine, K. P.: Effects of anthropogenic emissions on tropospheric ozone and its radiative forcing, Journal of Geophysical Research, 102126, 101–28, https://doi.org/10.1029/97JD02226, 1997.

Bork, N., Elm, J., Olenius, T., and Vehkamäki, H.: Methane sulfonic acid-enhanced formation of molecular clusters of sulfuric acid and dimethyl amine, Atmospheric Chemistry and Physics, 14, 12 023–12 030, https://doi.org/10.5194/acp-14-12023-2014, 2014.

Boucher, O., Randall, D., Artaxo, P., Bretherton, C., Feingold, G., Forster, P., Kerminen, V.-m., Kondo, Y., Liao, H., Lohmann, U., Rasch, P., Satheesh, S., Sherwood, S., Stevens, B., and Zhang, X.: Clouds and aerosols, in: Climate Change 2013: The Physical Science Basis. Contribution of Working Group I to the Fifth Assessment Report of the Intergovernmental Panel on Climate Change, edited by Stocker, T., D. Qin, G.-K., Plattner, M., Tignor, S., Allen, J., Boschung, A., Nauels, Y., Xia, V., Midgley, B., and P.M., chap. 8, pp. 659–740, Cambridge University Press, Cambridge, United Kingdom and New York, NY, USA., 2013.

Carslaw, K. S., Lee, L. A., Reddington, C. L., Pringle, K. J., Rap, A., Forster, P. M., Mann, G. W., Spracklen, D. V., Woodhouse, M. T., Regayre, L. A., and Pierce, J. R.: Large contribution of natural aerosols to uncertainty in indirect forcing, Nature, 503, 67–71, https://doi.org/10.1038/nature12674, http://dx.doi.org/10.1038/nature12674, 2013.

Chameides, W. L., Fehsenfeld, F., Rodgers, M. O., Cardelino, C., Martinez, J., Parrish, D., Lonneman, W., Lawson, D. R., Rasmussen, R. A., Zimmerman, P., Greenberg, J., Mlddleton, P., and Wang, T.: Ozone precursor relationships in the ambient atmosphere, Journal of Geophysical Research, 97, 6037, https://doi.org/10.1029/91JD03014, http://doi.wiley.com/10.1029/91JD03014, 1992.

Charlsson, R. J., Lovelock, J., Andreae, M. O., and Warren, S. G.: Oceanic phytoplankton, atmospheric sulphur, cloud albedo and climate, Nature, 326, 1987.

Chin, M., Jacob, D. J., Gardner, G. M., Foreman-Fowler, M. S., Spiro, P. A., and Savoie, D. L.: A global three-dimensional model of tropospheric sulfate, Journal of Geophysical Research: Atmospheres, 101, 18 667–18 690, https://doi.org/10.1029/96JD01221, 1996.

Collins, J. W., Lamarque, J. F., Schulz, M., Boucher, O., Eyring, V., Hegglin, I. M., Maycock, A., Myhre, G., Prather, M., Shindell, D., and Smith, J. S.: AerChemMIP: Quantifying the effects of chemistry and aerosols in CMIP6, Geoscientific Model Development, 10, 585–607, https://doi.org/10.5194/gmd-10-585-2017, 2017.

Collins, W. J., Derwent, R. G., Johnson, C. E., and Stevenson, D. S.: The oxidation of organic compounds in the troposphere and their global warming potentials, Climatic Change, 52, 453–479, https://doi.org/10.1023/A:1014221225434, 2002.

Crutzen, P. and Lelieveld, J.: HUMAN IMPACTS ON ATMOSPHERIC CHEMISTY, Annual Review of Earth and Planetary Sciences, 29, 17–45, 2001.

Emmons, L. K., Walters, S., Hess, P. G., Lamarque, J.-F., Pfister, G. G., Fillmore, D., Granier, C., Guenther, A., Kinnison, D., Laepple, T., Orlando, J., Tie, X., Tyndall, G., Wiedinmyer, C., Baughcum, S. L., and Kloster, S.: Description and evaluation of the

Model for Ozone and Related chemical Tracers, version 4 (MOZART-4), Geoscientific Model Development Discussions, 3, 43–67, https://doi.org/10.5194/gmdd-2-1157-2009, 2010.

Gettelman, A.: Putting the clouds back in aerosol-cloud interactions, Atmospheric Chemistry and Physics, 15, 12 397–12 411, https://doi.org/10.5194/acp-15-12397-2015, 2015.

5 Gettelman, A. and Morrison, H.: Advanced two-moment bulk microphysics for global models. Part I: Off-line tests and comparison with other schemes, Journal of Climate, 28, 1268–1287, https://doi.org/10.1175/JCLI-D-14-00102.1, 2015.

Gettelman, A., Morrison, H., Santos, S., Bogenschutz, P., and Caldwell, P. M.: Advanced two-moment bulk microphysics for global models. Part II: Global model solutions and aerosol-cloud interactions, Journal of Climate, 28, 1288–1307, https://doi.org/10.1175/JCLI-D-14-00103.1, 2015.

10 Ghan, S. J.: Technical note: Estimating aerosol effects on cloud radiative forcing, Atmospheric Chemistry and Physics, 13, 9971–9974, https://doi.org/10.5194/acp-13-9971-2013, 2013.

Guenther, A. B., Jiang, X., Heald, C. L., Sakulyanontvittaya, T., Duhl, T., Emmons, L. K., and Wang, X.: The model of emissions of gases and aerosols from nature version 2.1 (MEGAN2.1): An extended and updated framework for modeling biogenic emissions, Geoscientific Model Development, 5, 1471–1492, https://doi.org/10.5194/gmd-5-1471-2012, 2012.

15 Hoose, C., Lohmann, U., Erdin, R., and Tegen, I.: The global influence of dust mineralogical composition on heterogeneous ice nucleation in mixed-phase clouds, Environmental Research Letters, 3, https://doi.org/10.1088/1748-9326/3/2/025003, 2008.

Hoose, C., Kristjánsson, J. E., Iversen, T., Kirkevåg, A., Seland, and Gettelman, A.: Constraining cloud droplet number concentration in GCMs suppresses the aerosol indirect effect, Geophysical Research Letters, 36, 1–5, https://doi.org/10.1029/2009GL038568, 2009.

Hoose, C., Kristjánsson, J. E., Chen, J.-P., and Hazra, A.: A Classical-Theory-Based Parameterization of Heterogeneous Ice Nucleation
20 by Mineral Dust, Soot, and Biological Particles in a Global Climate Model, Journal of the Atmospheric Sciences, 67, 2483–2503, https://doi.org/10.1175/2010JAS3425.1, 2010.

Iversen, T., Bentsen, M., Bethke, I., Debernard, J. B., Kirkevåg, A., Seland, Ø., Drange, H., Kristjánsson, J. E., Medhaug, I., Sand, M., and Seierstad, I. A.: The Norwegian Earth System Model, NorESM1-M – Part 2: Climate response and scenario projections, Geoscientific Model Development Discussions, 5, 2933–2998, https://doi.org/10.5194/gmdd-5-2933-2012, http://www.geosci-model-dev-discuss.net/
25 5/2933/2012/, 2013.

Jaenicke, R.: Natural Aerosols, Annals of the New York Academy of Sciences, 338, 317–329, https://doi.org/10.1111/j.1749-6632.1980.tb17129.x, 1980.

Khan, M. A. H., Cooke, M. C., Utembe, S. R., Archibald, A. T., Derwent, R. G., Xiao, P., Percival, C. J., Jenkin, M. E., Morris, W. C., and Shallcross, D. E.: Global modeling of the nitrate radical (NO3) for present and pre-industrial scenarios, Atmospheric Research, 164-165,
30 347–357, https://doi.org/10.1016/j.atmosres.2015.06.006, 2015.

Kirkevåg, A., Iversen, T., Seland, Ø., Debernard, J. B., Storelvmo, T., and Kristjánsson, J. E.: Aerosol-cloud-climate interactions in the climate model CAM-Oslo, Tellus, Series A: Dynamic Meteorology and Oceanography, 60 A, 492–512, https://doi.org/10.1111/j.1600-0870.2008.00313.x, 2008.

Kirkevåg, A., Iversen, T., Seland, Ø., Hoose, C., Kristjánsson, J. E., Struthers, H., Ekman, A. M. L., Ghan, S., Griesfeller, J., Nilsson, E. D.,
35 and Schulz, M.: Aerosol-climate interactions in the Norwegian Earth System Model – NorESM, Geoscientific Model Development Discussions, 5, 2599–2685, https://doi.org/10.5194/gmdd-5-2599-2012, 2013.

Kirkevåg, A., Grini, A., Olivié, D., Seland, Ø., Alterskjær, K., Hummel, M., Karset, I. H. H., Lewinchal, A., Xiaohong, L., Makkonen, R., Griesfeller, J., Schulz, M., and Iversen, T.: A production-tagged aerosol module for earth system models - extensions and updates for CAM5.3-Oslo/NorESM1.2. Manuscript in preperation, 2018.

Kooperman, G. J., Pritchard, M. S., Ghan, S. J., Wang, M., Somerville, R. C. J., and Russell, L. M.: Constraining the influence of natural variability to improve estimates of global aerosol indirect effects in a nudged version of the Community Atmosphere Model 5, Journal of Geophysical Research Atmospheres, 117, https://doi.org/10.1029/2012JD018588, 2012.

Lamarque, J. F., Bond, T. C., Eyring, V., Granier, C., Heil, A., Klimont, Z., Lee, D., Liousse, C., Mieville, A., Owen, B., Schultz, M. G., Shindell, D., Smith, S. J., Stehfest, E., Van Aardenne, J., Cooper, O. R., Kainuma, M., Mahowald, N., McConnell, J. R., Naik, V., Riahi, K., and Van Vuuren, D. P.: Historical (1850-2000) gridded anthropogenic and biomass burning emissions of reactive gases and aerosols: Methodology and application, Atmospheric Chemistry and Physics, 10, 7017–7039, https://doi.org/10.5194/acp-10-7017-2010, 2010.

Liu, X., Easter, R. C., Ghan, S. J., Zaveri, R., Rasch, P., Shi, X., Lamarque, J. F., Gettelman, A., Morrison, H., Vitt, F., Conley, A., Park, S., Neale, R., Hannay, C., Ekman, A. M., Hess, P., Mahowald, N., Collins, W., Iacono, M. J., Bretherton, C. S., Flanner, M. G., and Mitchell, D.: Toward a minimal representation of aerosols in climate models: Description and evaluation in the Community Atmosphere Model CAM5, Geoscientific Model Development, 5, 709–739, https://doi.org/10.5194/gmd-5-709-2012, 2012.

Liu, X., Ma, P. L., Wang, H., Tilmes, S., Singh, B., Easter, R. C., Ghan, S. J., and Rasch, P. J.: Description and evaluation of a new four-mode version of the Modal Aerosol Module (MAM4) within version 5.3 of the Community Atmosphere Model, Geoscientific Model Development, 9, 505–522, https://doi.org/10.5194/gmd-9-505-2016, 2016.

Lohmann, U.: Global anthropogenic aerosol effects on convective clouds in ECHAM5-HAM, Atmospheric Chemistry and Physics, 8, 2115–2131, https://doi.org/10.5194/acpd-7-14639-2007, 2008.

Lohmann, U.: Anthropogenic Aerosol Influences on Mixed-Phase Clouds, Current Climate Change Report, 3, 32–44, https://doi.org/10.1007/s40641-017-0059-9, 2017.

Lohmann, U. and Diehl, K.: Sensitivity Studies of the Importance of Dust Ice Nuclei for the Indirect Aerosol Effect on Stratiform Mixed-Phase Clouds, Journal of the Atmospheric Sciences, 63, 968–982, https://doi.org/10.1175/JAS3662.1, 2006.

Lohmann, U. and Ferrachat, S.: Impact of parametric uncertainties on the present-day climate and on the anthropogenic aerosol effect, Atmospheric Chemistry and Physics, 10, 11 373–11 383, https://doi.org/10.5194/acp-10-11373-2010, 2010.

Lohmann, U., Feichter, J., Penner, J., and Leaitch, R.: Indirect effect of sulfate and carbonaceous aerosols: A mechanistic treatment, Journal of Geophysical Research: Atmospheres, 105, 12 193–12 206, https://doi.org/10.1029/1999JD901199, http://doi.wiley.com/10.1029/1999JD901199, 2000.

Makkonen, R., Seland, Ø., Kirkevåg, A., Iversen, T., and Kristjánsson, J. E.: Evaluation of aerosol number concentrations in NorESM with improved nucleation parameterization, Atmospheric Chemistry and Physics, 14, 5127–5152, https://doi.org/10.5194/acp-14-5127-2014, 2014.

Menon, S. and Rotstayn, L.: The radiative influence of aerosol effects on liquid-phase cumulus and stratiform clouds based on sensitivity studies with two climate models, Climate Dynamics, 27, 345–356, https://doi.org/10.1007/s00382-006-0139-3, 2006.

Morrison, H. and Gettelman, A.: A new two-moment bulk stratiform cloud microphysics scheme in the community atmosphere model, version 3 (CAM3). Part I: Description and numerical tests, Journal of Climate, 21, 3642–3659, https://doi.org/10.1175/2008JCLI2105.1, 2008.

Murray, L. T., Mickley, L. J., Kaplan, J. O., Sofen, E. D., Pfeiffer, M., and Alexander, B.: Factors controlling variability in the oxidative capacity of the troposphere since the Last Glacial Maximum, Atmospheric Chemistry and Physics, 14, 3589–3622, https://doi.org/10.5194/acp-14-3589-2014, 2014.

Myhre, G., Shindell, D., Bréon, F.-M., Collins, W., Fuglestvedt, J., Huang, J., Koch, D., Lamarque, J.-F., Lee, D., Mendoza, B., Nakajima, T., Robock, A., Stephens, G., Takemura, T., and Zhang, H.: Anthropogenic and Natural Radiative Forcing, in: Climate Change 2013: The Physical Science Basis. Contribution of Working Group I to the Fifth Assessment Report of the Intergovernmental Panel on Climate Change, edited by Stocker, T., D. Qin, G.-K., Plattner, M., Tignor, S., Allen, J., Boschung, A., Nauels, Y., Xia, V., Midgley, B., and P.M., chap. 7, pp. 659–740, Cambridge University Press, Cambridge, United Kingdom and New York, NY, USA, https://doi.org/10.1017/CBO9781107415324.018, 2013.

Naik, V., Horowitz, L. W., Fiore, A. M., Ginoux, P., Mao, J., and Aghedo, A. M.: Impact of preindustrial to present-day changes in short-lived pollutant emissions on atmospheric composition and climate forcing, Journal of Geophysical Research Atmospheres, 118, 8086–8110, https://doi.org/10.1002/jgrd.50608, 2013a.

Naik, V., Voulgarakis, A., Fiore, A. M., Horowitz, L. W., Lamarque, J. F., Lin, M., Prather, M. J., Young, P. J., Bergmann, D., Cameron-Smith, P. J., Cionni, I., Collins, W. J., Dalsøren, S. B., Doherty, R., Eyring, V., Faluvegi, G., Folberth, G. A., Josse, B., Lee, Y. H., MacKenzie, I. A., Nagashima, T., Van Noije, T. P., Plummer, D. A., Righi, M., Rumbold, S. T., Skeie, R., Shindell, D. T., Stevenson, D. S., Strode, S., Sudo, K., Szopa, S., and Zeng, G.: Preindustrial to present-day changes in tropospheric hydroxyl radical and methane lifetime from the Atmospheric Chemistry and Climate Model Intercomparison Project (ACCMIP), Atmospheric Chemistry and Physics, 13, 5277–5298, https://doi.org/10.5194/acp-13-5277-2013, 2013b.

Neale, R. B., Chen, C.-C., Gettelman, A., Lauritzen, P. H., Park, S., Williamson, D. L., Conley, A. J., Garcia, R., Kinnison, D., Lamarque, J.-F., Marsh, D., Mills, M., Smith, A. K., Tilmes, S., Vitt, F., Morrison, H., Cameron-Smith, P., Collins, W. D., Iacono, M. J., Easter, R. C., Ghan, S. J., Liu, X., Rasch, P. J., and Taylor, M. A.: Description of the NCAR Community Atmosphere Model (CAM 5.0), 2012.

Neubauer, D., Lohmann, U., Hoose, C., and Frontoso, M. G.: Impact of the representation of marine stratocumulus clouds on the anthropogenic aerosol effect, Atmospheric Chemistry and Physics, 14, 11 997–12 022, https://doi.org/10.5194/acp-14-11997-2014, 2014.

Nightingale, P. D., Malin, G., Law, C. S., Watson, A. J., Liss, P. S., Liddicoat, M. I., Boutin, J., and Upstill-Goddard, R. C.: In situ evaluation of air-sea gas exchange parameterizations using novel conservative and volatile tracers, Global Biogeochemical Cycles, 14, 373–387, https://doi.org/10.1029/1999GB900091, 2000.

Oleson, K. W., Lawrence, D. M., Authors, L., Bonan, G. B., Drewniak, B., Huang, M., Koven, C. D., Levis, S., Li, F., Riley, W. J., Subin, Z. M., Swenson, S. C., Thornton, P. E., Bozbiyik, A., Fisher, R., Heald, C. L., Kluzek, E., Lamarque, J.-F., Lawrence, P. J., Leung, L. R., Lipscomb, W., Muszala, S., Ricciuto, D. M., Sacks, W., Sun, Y., Tang, J., and Yang, Z.-L.: Technical Description of version 4.5 of the Community Land Model (CLM), http://library.ucar.edu/research/publish-technote, 2013.

Pavelin, E. G., Johnson, C. E., Rughooputh, S., and Toumi, R.: Evaluation of pre-industrial surface ozone measurements made using Schonbein's method, Atmospheric Environment, 33, 919–929, https://doi.org/10.1016/S1352-2310(98)00257-X, 1999.

Pincus, R. and Baker, M. B.: Effect of precipitation on the albedo susceptibility of clouds in the marine boundary layer, Nature, 372, 250–252, 1994.

Prinn, R. G.: THE CLEANSING CAPACITY OF THE ATMOSPHERE, Annual Review of Environment and Resources, 28, 29–57, https://doi.org/10.1146/annurev.energy.28.011503.163425, 2003.

Salzmann, M., Ming, Y., Golaz, J. C., Ginoux, P. A., Morrison, H., Gettelman, A., Kramer, M., and Donner, L. J.: Two-moment bulk stratiform cloud microphysics in the GFDL AM3 GCM: Description, evaluation, and sensitivity tests, Atmospheric Chemistry and Physics, 10, 8037–8064, https://doi.org/10.5194/acp-10-8037-2010, 2010.

Sant, V., Posselt, R., and Lohmann, U.: Prognostic precipitation with three liquid water classes in the ECHAM5-HAM GCM, Atmospheric Chemistry and Physics, 15, 8717–8738, https://doi.org/10.5194/acp-15-8717-2015, 2015.

Seinfeld, J. H.: Urban Air Pollution: State of the Science, Science, 243, 745–752, https://doi.org/10.1126/science.243.4892.745, http://www.sciencemag.org/cgi/doi/10.1126/science.243.4892.745, 1989.

Seinfeld, J. H. and Pandis, S. N.: Atmospheric Chemistry and Physics: From Air Pollution to Climate Change, Wiley, third edit edn., 2016.

Shaw, S. L., Gantt, B., and Meskhidze, N.: Production and Emissions of Marine Isoprene and Monoterpenes: A Review, Advances in Meteorology, 2010, 1–24, https://doi.org/10.1155/2010/408696, http://www.hindawi.com/journals/amete/2010/408696/, 2010.

Storelvmo, T.: Aerosol Effects on Climate via Mixed-Phase and Ice Clouds, Annual Review of Earth and Planetary Sciences, 45, 199–222, https://doi.org/10.1146/annurev-earth-060115-012240, http://www.annualreviews.org/doi/10.1146/annurev-earth-060115-012240, 2017.

Storelvmo, T., Kristjánsson, J. E., Lohmann, U., Iversen, T., Kirkevåg, A., and Seland: Modeling of the wegener-bergeron-findeisen process - Implications for aerosol indirect effects, Environmental Research Letters, 3, https://doi.org/10.1088/1748-9326/3/4/045001, 2008.

Tie, X., Brasseur, G., Emmons, L., Horowitz, L., and Kinnison, D.: Effects of aerosols on tropospheric oxidants: A global model study, Journal of Geophysical Research: Atmospheres, 106, 22 931–22 964, https://doi.org/10.1029/2001JD900206, http://doi.wiley.com/10.1029/2001JD900206, 2001.

Tonttila, J., Jarvinen, H., and Raisanen, P.: Explicit representation of subgrid variability in cloud microphysics yields weaker aerosol indirect effect in the ECHAM5-HAM2 climate model, Atmospheric Chemistry and Physics, 15, 703–714, https://doi.org/10.5194/acp-15-703-2015, 2015.

Tsigaridis, K., Krol, M., Dentener, F. J., Balkanski, Y., Lathière, J., Metzger, S., Hauglustaine, D. A., and Kanakidou, M.: Change in global aerosol composition since preindustrial times, Atmospheric Chemistry and Physics, 6, 5143–5162, https://doi.org/10.5194/acp-6-5143-2006, 2006.

Twomey, S.: The Influence of Pollution on the Shortwave Albedo of Clouds, Journal of the Atmospheric Sciences, 34, 1149–1152, https://doi.org/10.1175/1520-0469(1977)034<1149:TIOPOT>2.0.CO;2, 1977.

Twomey, S.: Aerosols, clouds and radiation, Atmospheric Environment Part A, General Topics, 25, 2435–2442, https://doi.org/10.1016/0960-1686(91)90159-5, 1991.

Unger, N.: Human land-use-driven reduction of forest volatiles cools global climate, Nature Climate Change, 4, 907–910, https://doi.org/10.1038/nclimate2347, 2014.

Wang, M., Ghan, S., Ovchinnikov, M., Liu, X., Easter, R., Kassianov, E., Qian, Y., and Morrison, H.: Aerosol indirect effects in a multi-scale aerosol-climate model PNNL-MMF, Atmospheric Chemistry and Physics, 11, 5431–5455, https://doi.org/10.5194/acp-11-5431-2011, 2011.

Wang, Y. and Jacob, D. J.: Anthropogenic forcing on tropospheric ozone and OH since preindustrial times, JOURNAL OF GEOPHYSICAL RESEARCH, 103, 31,123–31,135, https://doi.org/10.1029/1998JD100004, 1998.

Wang, Y., Liu, X., Hoose, C., and Wang, B.: Different contact angle distributions for heterogeneous ice nucleation in the Community Atmospheric Model version 5, Atmospheric Chemistry and Physics, 14, 10 411–10 430, https://doi.org/10.5194/acp-14-10411-2014, 2014.

Wayne, R. P., Barnes, I., Biggs, P., Burrows, J. P., Canosa-Mas, C. E., Hjorth, J., Le Bras, G., Moortgat, G. K., Perner, D., Poulet, G., Restelli, G., and Sidebottom, H.: The nitrate radical: Physics, chemistry, and the atmosphere, Atmospheric Environment. Part A. General Topics, 25, 1–203, https://doi.org/10.1016/0960-1686(91)90192-A, 1991.

Williams, J., de Reus, M., Krejci, R., Fischer, H., and Ström, J.: Application of the variability-size relationship to atmospheric aerosol studies: estimating aerosol lifetimes and ages, Atmospheric Chemistry and Physics Discussions, 2, 43–74, https://doi.org/10.5194/acpd-2-43-2002, 2002.

Woodhouse, M. T., Carslaw, K. S., Mann, G. W., Vallina, S. M., Vogt, M., Halloran, P. R., and Boucher, O.: Low sensitivity of cloud condensation nuclei to changes in the sea-air flux of dimethyl-sulphide, Atmospheric Chemistry and Physics, 10, 7545–7559, https://doi.org/10.5194/acp-10-7545-2010, 2010.

Young, P. J., Archibald, A. T., Bowman, K. W., Lamarque, J.-F., Naik, V., Stevenson, D. S., Tilmes, S., Voulgarakis, A., Wild, O., Bergmann, D., Cameron-Smith, P., Cionni, I., Collins, W. J., Dalsøren, S. B., Doherty, R. M., Eyring, V., Faluvegi, G., Horowitz, L. W., Josse, B., Lee, Y. H., MacKenzie, I. A., Nagashima, T., Plummer, D. A., Righi, M., Rumbold, S. T., Skeie, R. B., Shindell, D. T., Strode, S. A., Sudo, K., Szopa, S., and Zeng, G.: Pre-industrial to end 21st century projections of tropospheric ozone from the Atmospheric Chemistry and Climate Model Intercomparison Project (ACCMIP), Atmospheric Chemistry and Physics, 13, 2063–2090, https://doi.org/10.5194/acp-13-2063-2013, 2013.

Yun, Y. and Penner, J. E.: An evaluation of the potential radiative forcing and climatic impact of marine organic aerosols as heterogeneous ice nuclei, Geophysical Research Letters, 40, 4121–4126, https://doi.org/10.1002/grl.50794, 2013.

Zhang, K., Wan, H., Liu, X., Ghan, S. J., Kooperman, G. J., Ma, P. L., Rasch, P. J., Neubauer, D., and Lohmann, U.: Technical note: On the use of nudging for aerosol-climate model intercomparison studies, Atmospheric Chemistry and Physics, 14, 8631–8645, https://doi.org/10.5194/acp-14-8631-2014, 2014.
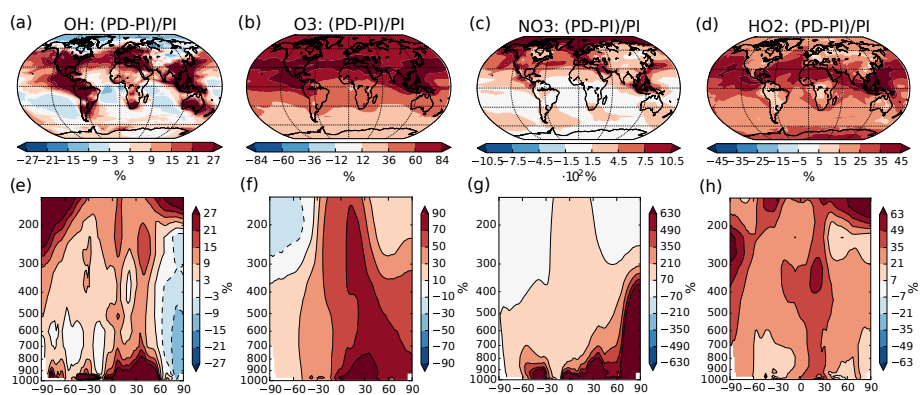
Figure 1. Percent change in the annual mean oxidant mixing ratio (mol/mol) between PI and PD in the dataset from Lamarque et al. (2010) used in this study. Top: mean change from surface and up to 550 hPa. Bottom: zonal mean change. Please note the different scales on the color bars.
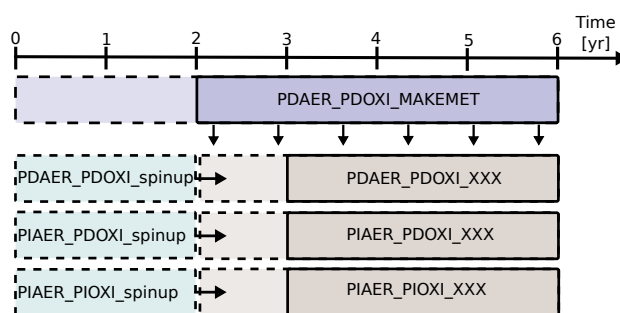
Figure 2. Overview of how the simulations were carried out. PDAER_PDOXI_MAKEMET produced meteorology for the other simulations from its last four years. Dashed lines show the part of the simulations used as spin up. Horizontal arrows show that the cases to the right of the arrow restarted from the already spun up case to the left. The spin up cases were not nudged, but started with free running meteorology from the same state as PDAER_PDOXI_MAKEMET. XXX refers to either ORG (original model setup), or the name of the sensitivity tests described in Sect. 3.2 and 4.3
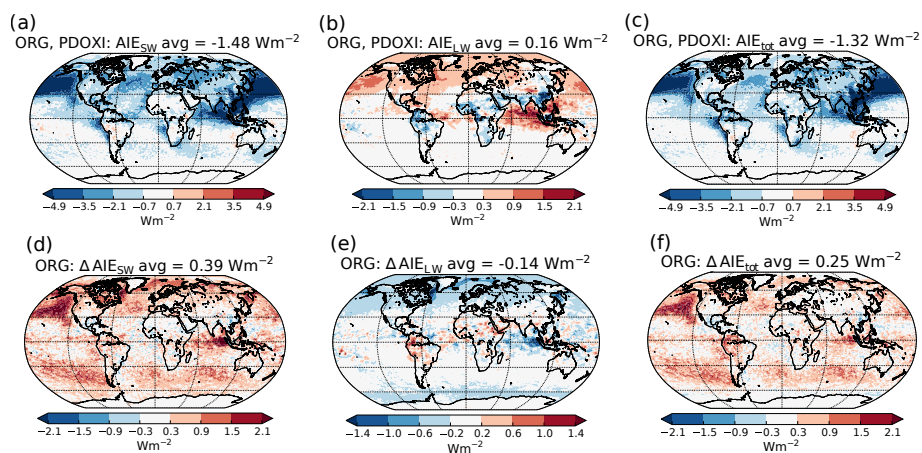
Figure 3. Top: PD-PI aerosol indirect effect when using the standard setup with PD-oxidants in both simulations. Left: shortwave, middle: longwave, right: total. Bottom: Differences in the PD-PI indirect effects between simulations performed with PI- and PD-oxidants in the PI-simulation.
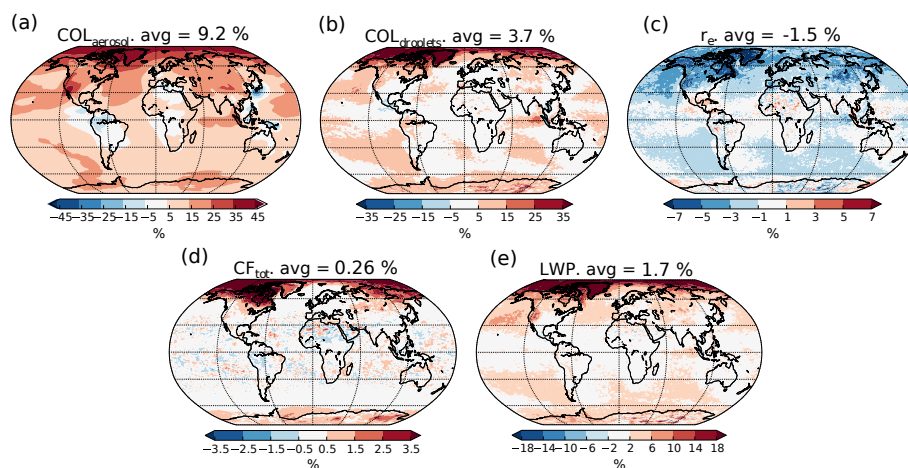
Figure 4. Relative change in aerosol and cloud properties in the PI-simulation when switching from PD- to PI-oxidants. (a) Column number of aerosols, (b) column number of cloud droplets, (c) effective radius of cloud droplets in the cloud top layer, (d) total cloud fraction, and (e) total gridbox averaged liquid water path.
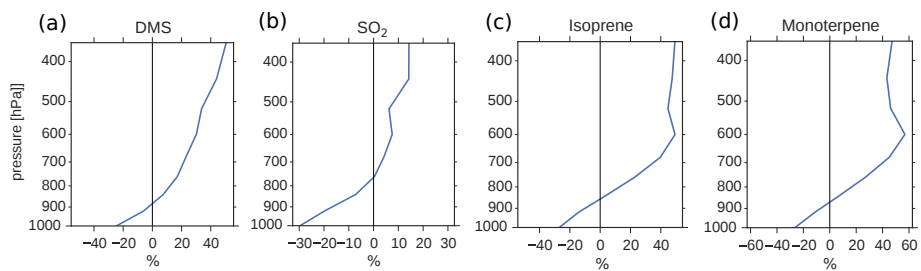
Figure 5. Global mean relative change in chemical loss of (a) DMS, (b) SO$_2$, (c) isoprene and (d) monoterpene when switching from PD- to PI-oxidants in the PI-simulation.
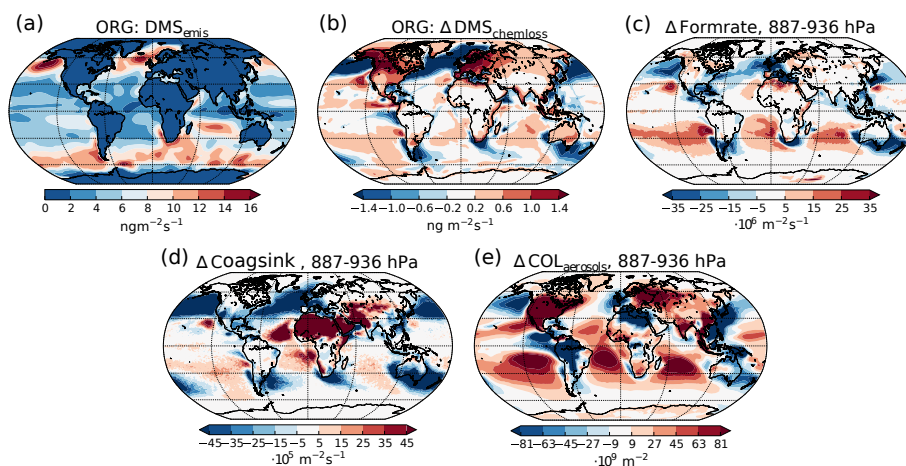
Figure 6. (a) Emission rate of DMS (same for both PI-simulations). (b) Difference in net chemical loss of DMS though oxidation (c) Difference in aerosol formation rate in the layer 887-936 hPa. (d) Difference in the coagulation sink during nucleation in the layer 887-936 hPa. (e) Difference in column burden of aerosols in the layer 887-936 hPa. All differences show values from the PI-simulation using PI-oxidants minus values from the PI-simulation using PD-oxidants.
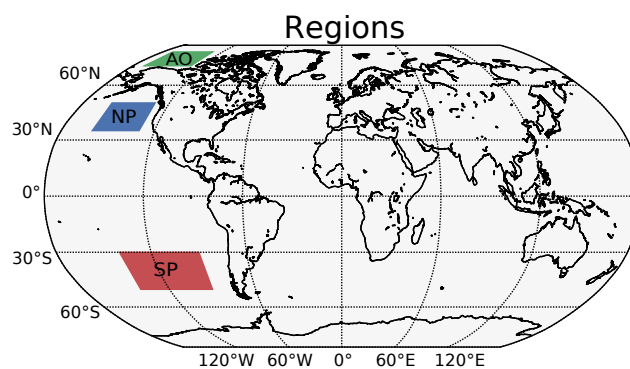
Figure 7. Selected regions with extra focus. AO: Arctic Ocean (70° N - 82° N, 130° W - 170° W). NP: North Pacific (35° N - 50° N, 130° W - 160° W). SP: South Pacific (30° S - 50° S, 90° W - 140° W).
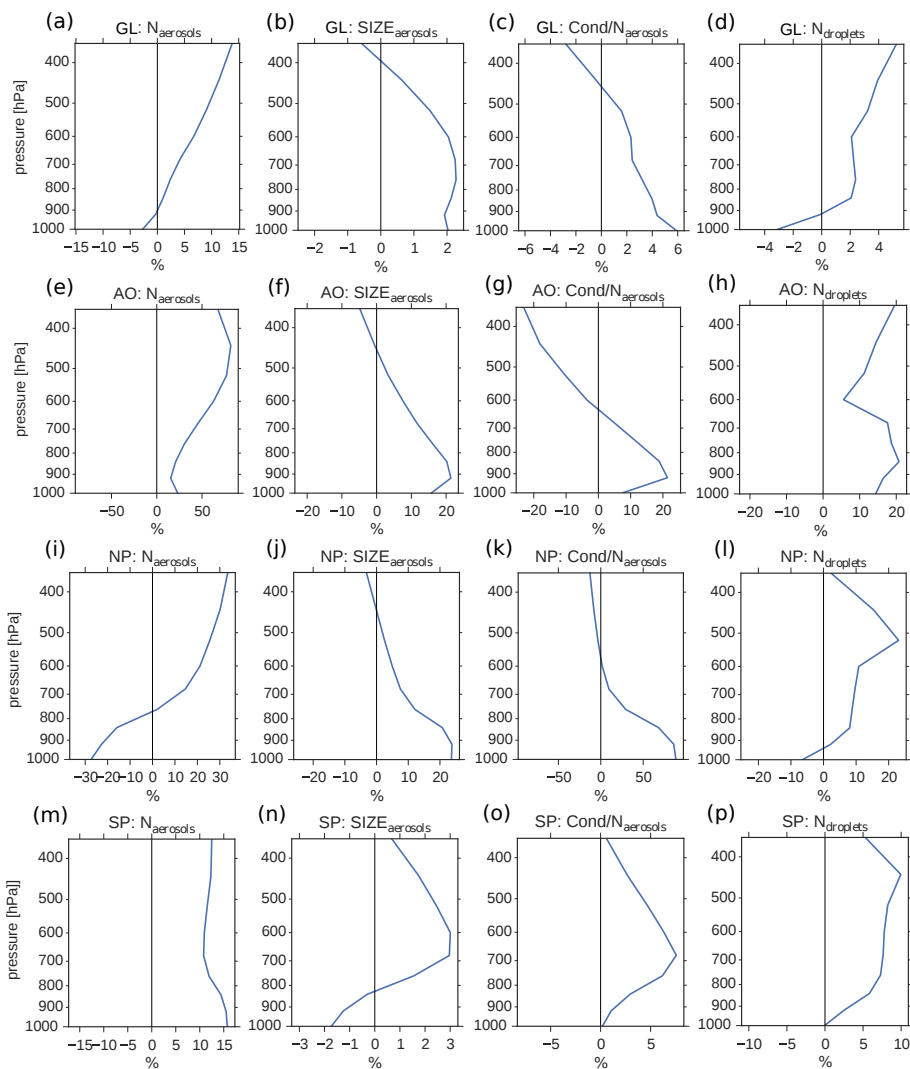
Figure 8. Vertical profiles of annual averaged changes in aerosol number concentration (left), aerosol size (middle left), aerosol condensate divided by the aerosol number concentration (middle right) and CDNC (right) on a global mean (GL) and in the three different regions from Fig. 7: Arctic Ocean (AO), North Pacific (NP) and South Pacific (SP), when switching from PD- to PI-oxidants in the PI simulation.
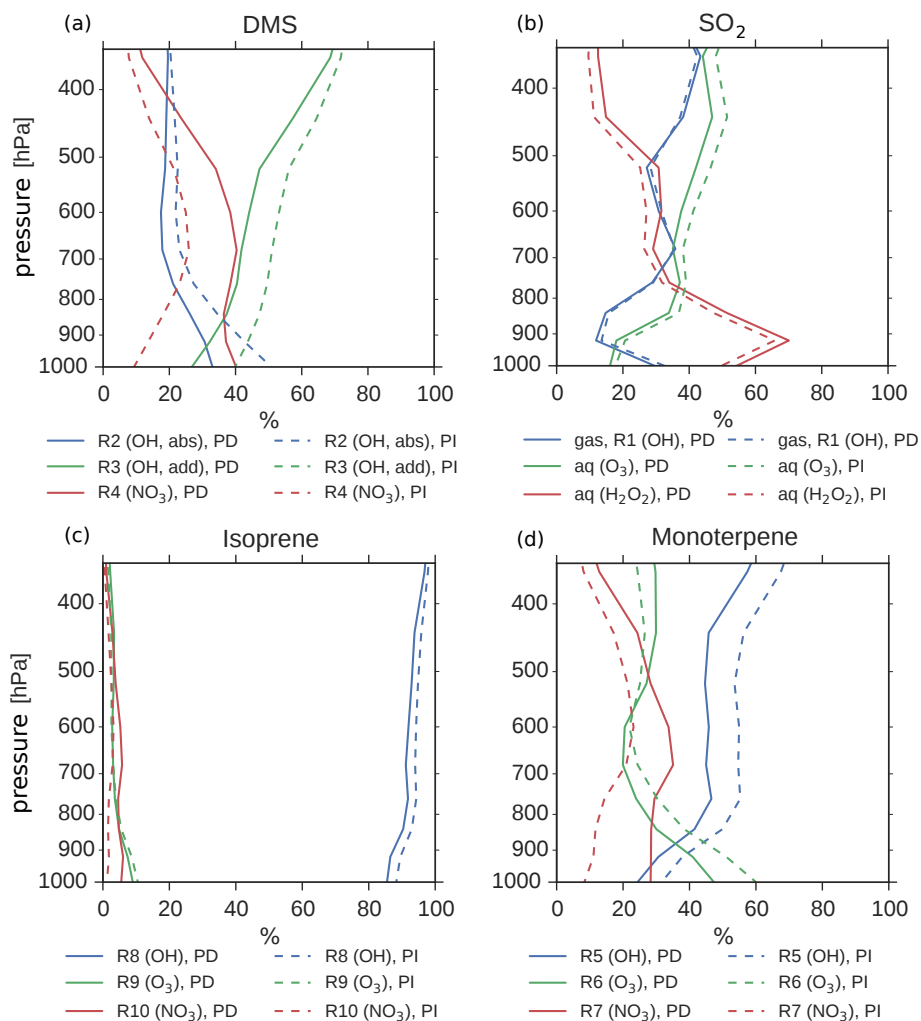
Figure 9. The importance of different oxidant reactions at different levels for (a) DMS, (b) SO_2 (c) isoprene and (d) monoterpene. Solid lines: PD-oxidants. Dashed lines: PI-oxidants. The value of a curve at a specific height tells how many percent of the oxidant reactions of that specie happening though the specified reaction. The sum of the three reactions at each level is equal to 100 % in each era.
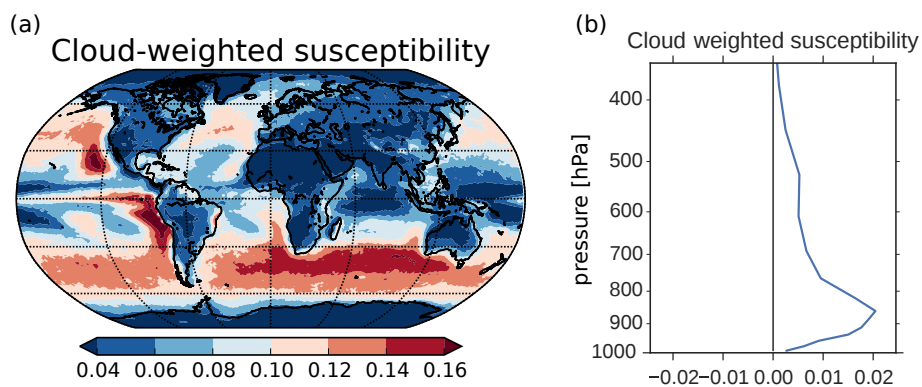
Figure 10. (a) Cloud-weighted susceptibility using Eq. (6) in Alterskjær et al. (2012). Cloud droplet size and numbers from the cloud top layer and the total cloud fraction were applied. (b) Vertical profile of the global mean cloud-weighted susceptibility.
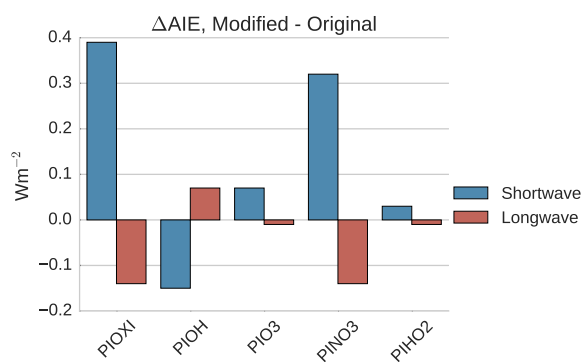
Figure 11. Differences in global mean shortwave and longwave aerosol indirect effect between the setups with modified PI-simulations (PIOXI, PIOH, PINO3 and PIHO2) and the original setup.
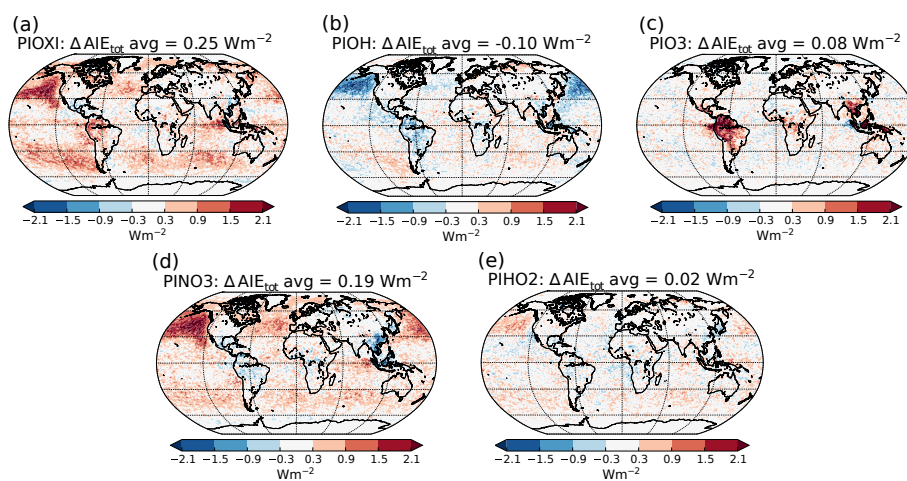
Figure 12. Differences in total aerosol indirect effect between the PI-simulation with (a) PIOXI, (b) PIOH, (c) PIO3, (d) PINO3, (e) PIHO2 and the original PI-simulation with only PD-oxidants.

Table 1. Chemical reactions with corresponding rate coefficients. For (R1), $fc = 3 \cdot 10^{-31} \cdot \left(\frac{300}{T}\right)^{3.3}$, and $ko = \frac{fc \cdot M}{1 + (fc \cdot M \cdot 1.5 \cdot 10^{12})}$, where M is all molecules that can act as a third body [cm^{-3}]. If the model does not trace an end product of a chemical reaction, the product is lost in the model and not written down in this table, explaining why the stochemetry is not exact in all of the reactions.

Reaction number	Reaction	Rate coefficient [cm^{3}molecule^{-1}s^{-1}]
(R1)	$SO_2 + OH + M \rightarrow H_2SO_4 + M$	$ko \cdot 0.6^{\left(1 + \left(\log_{10}(fc \cdot M \cdot 1.5 \cdot 10^{12})\right)^2\right)^{-1}}$
(R2)	$DMS + OH \rightarrow SO_2$	$9.6 \cdot 10^{-12} \cdot e^{-234/T}$
(R3)	$DMS + OH \rightarrow 0.75 \cdot SO_2 + 0.5 \cdot HO_2 + 0.029 \cdot SOA_{LV} + 0.114 \cdot SOA_{SV}$	$\frac{\left(1.7 \cdot 10^{-42} \cdot e^{7810/T}[O_2]\right)}{\left(1 + 5.5 \cdot 10^{-31} e^{7460/T}[O_2]\right)}$
(R4)	$DMS + NO_3 \rightarrow SO_2 + HNO_3$	$1.9 \cdot 10^{-13} \cdot e^{-520/T}$
(R5)	$monoterpene + OH \rightarrow 0.15 \cdot SOA_{SV}$	$1.2 \cdot 10^{-11} \cdot e^{-440/T}$
(R6)	$monoterpene + O_3 \rightarrow 0.15 \cdot SOA_{LV}$	$8.05 \cdot 10^{-16} \cdot e^{-640/T}$
(R7)	$monoterpene + NO_3 \rightarrow 0.15 \cdot SOA_{SV}$	$1.2 \cdot 10^{-12} \cdot e^{-490/T}$
(R8)	$isoprene + OH \rightarrow 0.05 \cdot SOA_{SV}$	$2.7 \cdot 10^{-11} \cdot e^{-390/T}$
(R9)	$isoprene + O_3 \rightarrow 0.05 \cdot SOA_{SV}$	$1.03 \cdot 10^{-14} \cdot e^{-1995/T}$
(R10)	$isoprene + NO_3 \rightarrow 0.05 \cdot SOA_{SV}$	$3.15 \cdot 10^{-12} \cdot e^{-450/T}$
(R11)	$HO_2 + HO_2 \rightarrow H_2O_2$	$\left(3.5 \cdot 10^{-13} \cdot e^{430/T} + 1.7 \cdot 10^{-33} \cdot e^{1000/T}\right)$ $\cdot \left(1 + 1.4 \cdot 10^{-21} \cdot [H_2O] \cdot e^{2200/T}\right)$
(R12)	$H_2O_2 + OH \rightarrow H_2O_2 + HO_2$	$2.9 \cdot 10^{-12} \cdot e^{-160/T}$
(R13)	$H_2O_2 + h\nu \rightarrow$	

Table 2. Overview of the prescribed precursor- and aerosol emissions and prescribed oxidant concentrations used in the three different simulations that were carried out for each modification to the default model setup.

Name of simulations	Prescribed emissions of aerosols and precursor gases	Prescribed concentrations of oxidants	SSTs, sea-ice extent, greenhouse gases and land use
PDAER_PDOXI_XXX	PD	PD	PD
PIAER_PDOXI_XXX	PI	PD	PD
PIAER_PIOXI_XXX	PI	PI	PD

Table 3. Global mean lifetime of different gaseous and aerosol species (g: gas, a: aerosol) when applying PD- to PI-oxidants in the PI-simulation. The lifetime is calculated as (Global mean burden)/(Global mean net loss).

Species	Lifetime, PD [h]	Lifetime, PI [h]	Change in lifetime [%]
SO_2 (g)	29	34	+17
DMS (g)	36	55	+53
Isoprene (g)	3.2	6.0	+88
Monoterpene (g)	2.6	5.3	+104
H_2SO_4 (g)	0.91	1.0	+9.9
SOA_{LV} (g)	0.65	0.82	+26
SOA_{SV} (g)	0.75	1.0	+9.9
SO_4 (a)	78	84	+7.7
SOA (a)	115	116	+0.9

Table 4. Difference in global mean SW and LW indirect effects between setups with the modified PI-simulation in the second column and the default PI-simulation with PD-oxidants. The bottom row shows the effect of changing all of the oxidants at a time (similar to Figure 3(c,d)), the other odd numbered rows show the effect of changing one oxidant at a time in the PI-simulation, while the even numbered rows show the difference in switching all oxidants (PIOXI) and all but one (PIOXI_PDXXX) in the PI-simulation.

Row number	Description of the modified PI-simulation	Change in shortwave aerosol indirect effect [Wm^{-2}]	Change in longwave aerosol indirect effect [Wm^{-2}]
1	PDOXI_PIOH	-0.15	+0.07
2	PIOXI − PIOXI_PDOH	-0.06	+0.02
3	PDOXI_PIO3	+0.07	-0.01
4	PIOXI − PIOXI_PDO3	+0.12	0.00
5	PDOXI_PINO3	+0.32	-0.14
6	PIOXI − PIOXI_PDNO3	+0.41	-0.11
7	PDOXI_PIHO2	+0.03	-0.01
8	PIOXI − PIOXI_PDHO2	+0.03	+0.01
9	PIOXI	+0.39	-0.14

Table 5. Information about how the setup for the sensitivity tests deviate from the default original setup.

Name of simulations	Description of setup
NOSOALVDMS	None of the SOA produced through (R3) was allowed to nucleate new particles. (R3) is thus replaced with $$DMS + OH \rightarrow 0.75 \cdot SO_2 + 0.5 \cdot HO_2 + 0.143 \cdot SOA_{SV}$$
NOSOALVBVOC	None of the SOA produced through (R6) was allowed to nucleate new particles. (R6) is thus replaced with $$monoterpene + O_3 \rightarrow 0.15 \cdot SOA_{SV}$$
NOSOA	No SOA production from DMS-oxidation. (R3) is thus replaced with $$monoterpene + O_3 \rightarrow 0.15 \cdot SOA_{SV}$$
NACTOFF	Activation from particle mixture number 1 (Kirkevåg et al., 2018) turned off. This mixture corresponds to the nucleation mode in modal aerosol schemes, and this is where we find the newly formed SOA- and SO_4-aerosols.